

# Spin-polarized electron transport in hybrid graphene-BN nanoribbons

Song Gao<sup>1</sup>, Wei Lu<sup>1</sup>, Guo-Hui Zheng<sup>1</sup>, Yalei Jia<sup>1</sup>, and San-Huang Ke<sup>1,2,\*</sup>

<sup>1</sup>MOE Key Laboratory of Microstructured Materials, School of Physics Science and Engineering, Tongji University, 1239 Siping Road, Shanghai 200092, P.R. China

<sup>2</sup>Beijing Computational Science Research Center, 10 Dongbeiwang West Road, Beijing 100094, P.R. China

E-mail: \*shke@tongji.edu.cn

**Abstract.** The experimental realization of hybrid graphene and h-BN provides a new way to modify the electronic and transport properties of graphene-based materials. In this work, we investigate the spin-polarized electron transport in hybrid graphene-BN zigzag nanoribbons by performing first-principles nonequilibrium Green's function method calculations. A 100% spin-polarized electron transport in a large energy window around the Fermi level is found and this behavior is independent of the ribbon width as long as there contain 3 zigzag carbon chains. This behavior may be useful in making perfect spin filters.

## 1. Introduction

In recent years, graphene and monolayer hexagonal boron nitride (h-BN) have been attracted much attention for their potential applications in next-generation electronics[1, 2, 3, 4, 5] after they were successfully synthesized in experiments by different methods[6, 7, 8, 9]. Zigzag-edged graphene nanoribbons (zGNRs) exhibit spin-polarized edge states which are localized around the two edges, as have been observed in monatomic step edges of graphite by scanning probe techniques[11, 12]. While the zigzag-edged h-BN nanoribbons (zBNNRs) are found to be spin degenerated except for bare ones[13]. Experimentally, people have demonstrated the ability to make graphene-BN stacks[14] as well as domain hybridized layers[10]. Very recently, Sutter et al. studied the growth and interface formation of monolayer graphene-BN heterostructures on ruthenium substrates by using a combination of in situ microscopy techniques[15]. All these advances in hybridizing conducting graphene with insulating h-BN offer a new scheme to tune the electronic properties of these low-dimensional materials.

Over the past few years, the electronic and transport properties of GNRs modified with BN domains or BNNRs have been investigated extensively. For instance, people successfully tuned the band gap of GNRs by introducing BN domains or BNNRs[16, 17, 18]. Furthermore, several approaches have been proposed to control the spin transport in GNR/BNNR hybrid systems, which may be useful in spintronics. Dong et al. found that a BNNR seamlessly connected between two pieces of GNRs can result in 100% electron spin polarization[18]. He et al. found that the currents with different spin configurations display different behavior for hybridized zBNNR<sub>m</sub>-zGNR<sub>n</sub> systems with certain  $n$  [16], but they did not find a way to achieve 100% spin polarization. Calculations by Dubois et al. showed that an erect heterojunction made of a bare zBNNR and zGNR can be a passive spin filter[19].

We note that highly spin-polarized electron transport may be produced by destroying the spin symmetry of zGNRs as in the case of parallel hybrid zGNR/zBNNR systems. In this work, we investigate



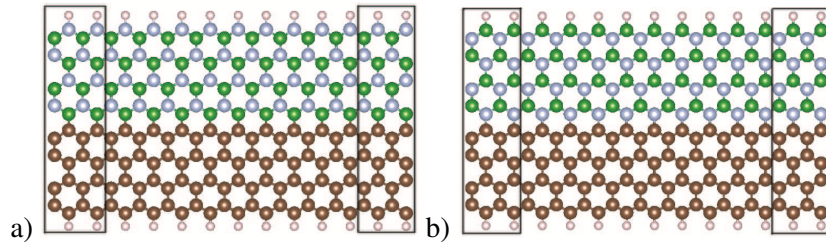


**Figure 1.** (Color online) Structures of hybrid systems of 4-zGNR/4-zBNNR. (a) C atoms are connected to B atoms, (b) C atoms are connected to N atoms. The brown, pink, gray, and green balls denote the C, H, N, and B atoms, respectively.

the electron transport properties of the parallel hybrid zGNR/zBNNR systems with different widths by performing first-principles calculations based on the nonequilibrium Green's function (NEGF) method combined with the density functional theory (DFT). Two different cases are considered: The zGNR is connected to the zBNNR via B and N atoms, respectively. It is found that highly spin-polarized electron transport in a large energy window around the Fermi level is presented. Especially, a 100% spin-polarized transport appears, which is independent of the ribbon width as long as there contain 3 zigzag carbon chains in the zGNR.

## 2. Models and Computation

We first consider a zGNR consisting of 8 zigzag carbon chains (8-zGNR). Then we gradually substitute these carbon chains with BN chains to construct parallel zGNR/zBNNR hybrid nanoribbon systems. The connection is made via the B atoms (system A) or N atoms (system B). The two systems are denoted by  $mBn$  and  $mNn$ , respectively, with  $m$  and  $n$  being the numbers of C chains and BN chains, respectively. The two edges of the hybrid nanoribbons are saturated by H atoms. As an example, the structures of the 4B4 and 4N4 nanoribbons are shown in Fig.1. There is a spin-polarized edge state localized around the edge of the zGNR and we choose its spin state as spin majority ( $\alpha$ -spin) (This can always be realized by, for example, applying an external magnetic field[20]). To investigate the electron transport through the nanoribbon systems, we adopt the NEGF method combined with first-principles DFT calculations[21]. The periodic nanoribbon systems are divided artificially into three subsystems: left lead, scattering region, and right lead (see Fig.1). The self-consistent Kohn-Sham Hamiltonian of the scattering region and the self-energies of two semi-infinite leads are used to construct a single-particle Green's function from which the transmission coefficient at any energy is calculated. The computational techniques have been described in details previously[21]. For the DFT electronic structure calculations, we employ a double- $\zeta$  plus polarization (DZP) numerical basis set for all atomic species[22, 23]. The optimized Troullier-Martins pseudopotentials[24] are adopted to describe the atomic cores and the PBE version of the generalized gradient approximation (GGA)[25] is used for the electron exchange and correlation. The atomic structures of the systems studied are fully optimized by minimizing the forces on atoms to be smaller than 0.005 eV/Å.

## 3. Results and Analyses

To begin with, we present the transmission functions of pristine 8-zGNR with ferromagnetic (FM) and antiferromagnetic (AFM) spin configurations, as shown in Fig.2. For the FM configuration (see Fig.2(a)), the system is metallic and there is one  $\alpha$  channel and one  $\beta$  channel around the Fermi energy. Away from the Fermi energy, there is an  $\alpha$  plateau around -0.3eV and a  $\beta$  plateau around 0.25eV, which is consistent with the spin-polarized band structure shown in Fig.2(c). For the AFM configuration (see Fig.2(b)), the two spins are degenerate and the system becomes semiconducting with a band gap of about 0.5eV, which is consistent with the spin-unpolarized band structure shown in Fig.2(d). These results agree well with a

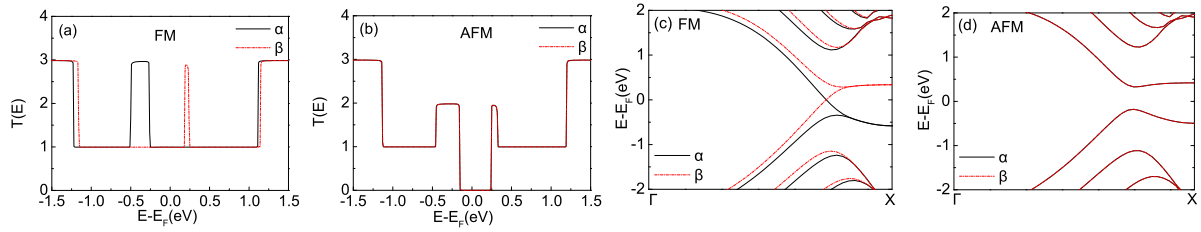


**Figure 2.** (Color online) Transmission functions of pristine 8-zGNR with (a) FM spin configuration and (b) AFM spin configuration. (c)(d) Band structures of 8-zGNR with FM and AFM configuration, respectively.

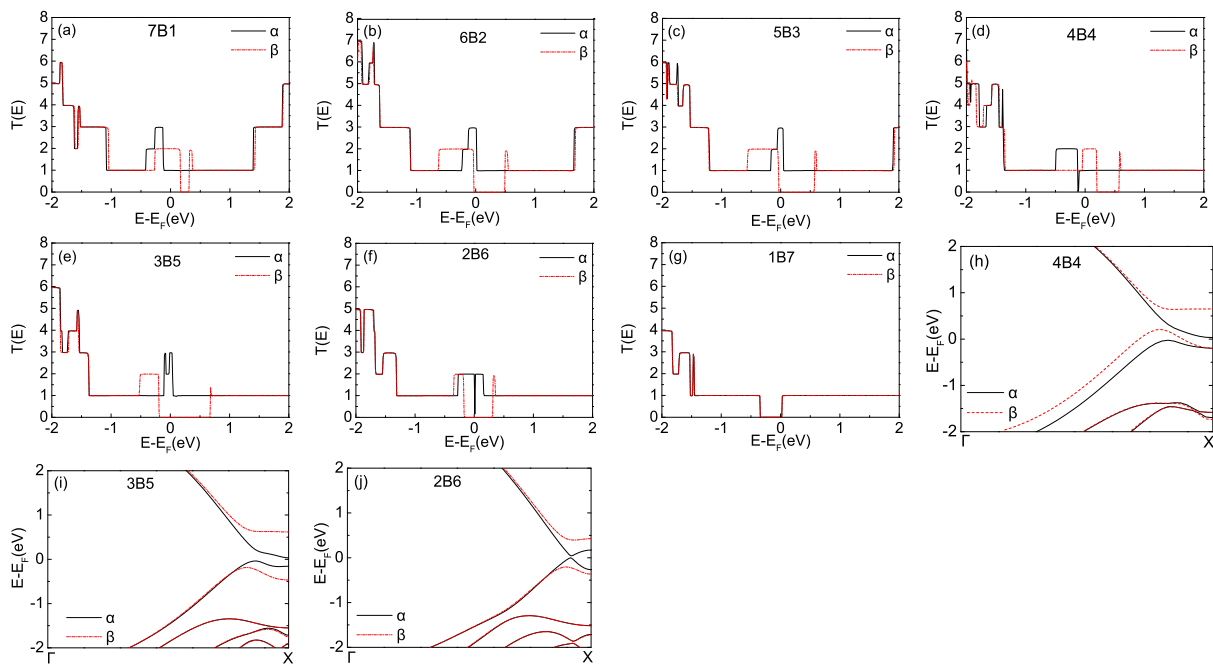


**Figure 3.** (Color online) (a)-(g) Transmission functions of different hybrid nanoribbons (from 7B1 to 1B7). (h)-(j) Band structures of 4B4, 3B5, and 2B6.

previous work about the transport in pristine 8-zGNRs[26].

Now, let us look at the transport properties of system A (connected via B atoms). The calculated transmission functions ( $T(E)$ ) are given in Figs.3(a)-(g). The first thing to note is the significant spin polarization around the Fermi energy for all cases calculated. When the width of BN doesn't exceed half of the ribbon width (from 7B1 to 4B4), the  $\alpha$ -spin shows the analogous behavior of pristine 8-zGNR with FM configuration while the  $\beta$ -spin shows the analogous behavior of pristine 8-zGNR with AFM configuration except for the fact that the Fermi level is shifted to lower energies for the two spins (see Figs.3 (a)-(d) vs Fig.2).

To understand the special transport properties, we calculate the band structures of these systems. Our calculation shows that their band structures (from 7B1 to 4B4) are similar, therefore, we take the band structure of 4B4 as an example to analyze (see Fig.3(h)). One can find that the  $\alpha$ -spin band and  $\beta$ -spin band show indeed analogous behavior to those of the pristine 8-zGNR with FM and AFM spin configuration, respectively.

When the width of BN exceeds half of the ribbon width (from 3B5 to 1B7, see Fig.3(e)-(g)), the

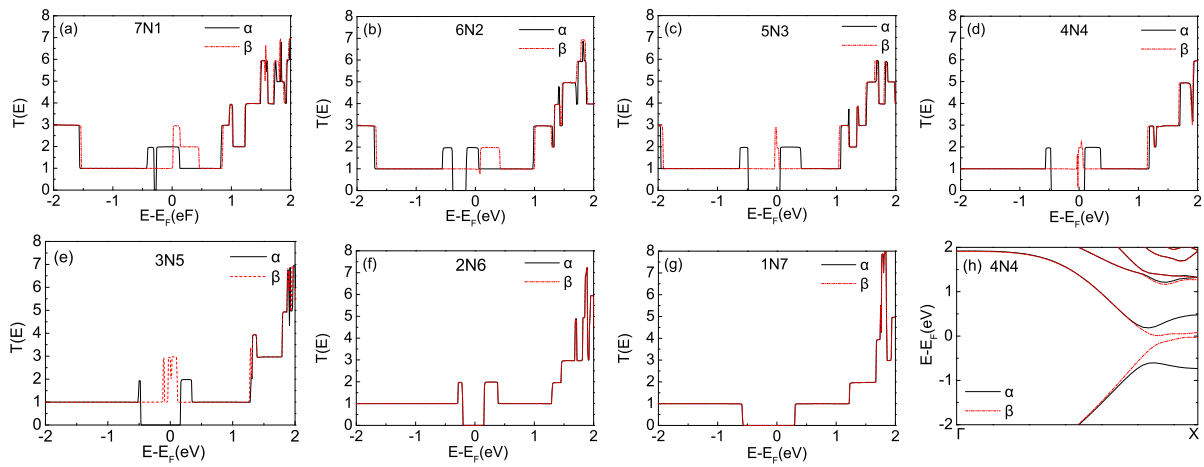


**Figure 4.** (Color online) (a)-(g) Transmission functions of different hybrid nanoribbons (from 7N1 to 1N7). (h) The band structure of 4N4.

Fermi level moves back to the transport gap for the  $\beta$ -spin. As a result, for 3B5 and 2B6 there comes a complete (100%) spin polarization in a large energy range around the Fermi level as shown in Fig.3 (e)-(f). This can also be seen clearly in the band structures of 3B5 and 2B6 shown in Fig.3 (i) and (j): The Fermi level is in the band gap of the  $\beta$ -spin, where the  $\alpha$ -spin bands exist. As for 1B7, that is, there is only one zigzag carbon chain presented in the ribbon, the spin polarization disappears leaving a transmission gap around the Fermi level (see Fig.3 (g)).

Next, let us look at the transport behavior of system B (from 7N1 to 1N7) as shown in Fig.4. One can see that the behavior is quite different from system A: Now the  $\alpha$ -spin shows the analogous behavior of pristine 8-zGNR with AFM configuration while the  $\beta$ -spin shows the analogous behavior of pristine 8-zGNR with FM configuration, just being opposite to system A. This can also be seen in the band structure of 4N4 shown in Fig.4 (h) for example: In contrary to 4B4, here the  $\alpha$ -spin bands show the behavior of pristine 8-zGNR with AFM configuration while  $\beta$ -spin bands show the behavior of pristine 8-zGNR with FM configuration. In the case of 3N5, a 100% spin polarization appears within the energy window of  $(-0.50, 0.16)$  eV as shown in Fig.4 (e). In this energy window the  $\alpha$ -spin channel is completely blocked while there come large transmission coefficients for the  $\beta$ -spin channel. As for the 2N6 and 1N7 systems, the spin polarization disappears (see Figs.4 (f) and (g)) leaving a transport gap of 0.3 and 0.9 eV, respectively. This provides a reliable way to modifying largely the band gap of the hybrid nanoribbons.

As mentioned above, the transport properties of 3B5 and 3N5 is very interesting. Both of them can provide a large energy windows around the Fermi level where the electron transport is 100% spin polarized and, therefore, may be used to produce high-performance spin filters. To check whether or not this behavior is general for hybrid nanoribbons consisting of 3 zigzag carbon chains, we further calculate other systems with different ribbon widths: 3B1, 3B3, 3B7, and 3N1, 3N3, 3N7. The transmission functions are given in Fig.5. As it can be seen, in all the cases there exists the energy window of 100% spin polarization. Furthermore, the range of this energy window increases gradually with increasing ribbon width, indicating that this behavior is general for hybrid zGNR/zBNNR systems consisting of 3 zigzag carbon chains.

To understand this 100% spin polarization, we analyze the band structure and projected density of states (PDOS) of 3N5, as shown in Fig.6. There is a band gap for the  $\alpha$ -spin energy bands which are just analogous with the band structure of pristine 8-zGNR with AFM configuration. However, for the  $\beta$ -spin the band gap disappears. The PDOS indicates that the two bands in the  $\alpha$ -spin band gap come from the hybridization of  $p_z$  orbital of C atoms and  $p_z$  orbital of N atoms, indicating that the complete spin polarization effect stems from the interaction between the GNR and BNNR.

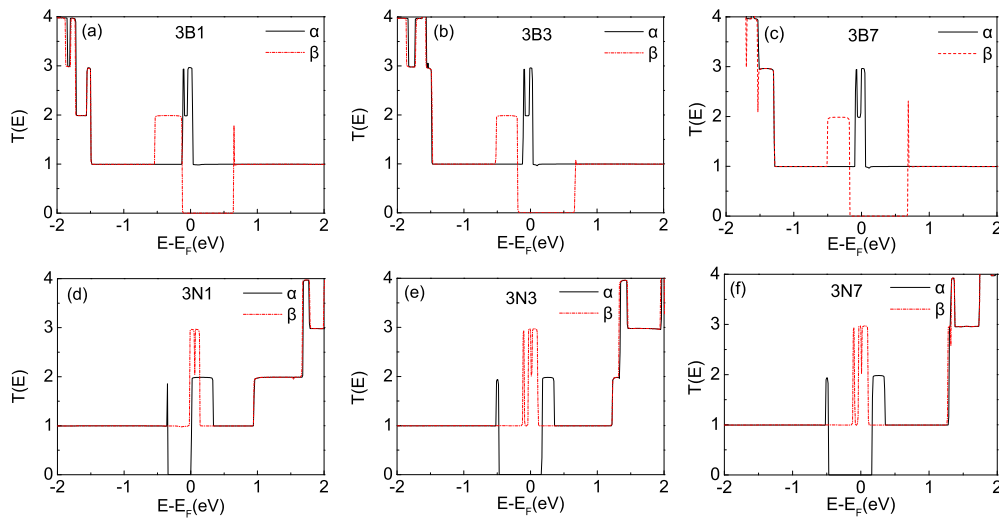


**Figure 5.** (Color online) Transmission functions of (a) 3B1, (b) 3B3, (c) 3B7, and (d) 3N1, (e) 3N3, (f) 3N7.

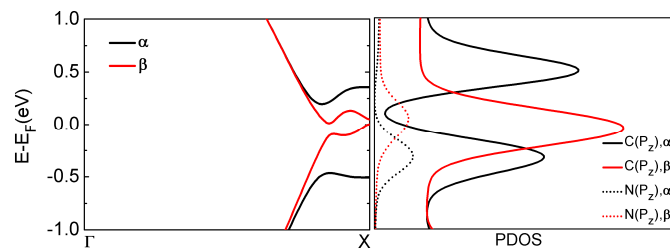


**Figure 6.** (Color online) The band structure and PDOS of 3N5.

#### 4. Conclusions

By performing first-principles calculations based on the nonequilibrium Green's function method combined with density functional theory, we have studied the electron transport behavior in hybrid zGNR/zBNR nanoribbons with different connection atoms and ribbon widths, which can be now fabricated in experiments. Significant spin-polarized transport behavior is found in most cases. Especially, hybrid nanoribbons consisting of 3 zigzag carbon chains will provide a large energy window around the Fermi level where the electron transport is 100% spin polarized. This is a general behavior regardless of the connection atoms (B or N atom) and the ribbon width. This behavior may be used in making perfect spin filters.

#### 5. Acknowledgments

This work was supported by the National Natural Science Foundation of China under Grants No. 11174220 and 11374226.

#### References

- [1] A. K. Geim, 1992 Science **324**, 1530.
- [2] A. H. Castro Neto, F. Guinea, K. S. Novoselov and A. K. Geim, 2009 Rev. Mod. Phys **81**, 183.
- [3] A. Nad, K. Raidongia, K. P. S. S. Hembram, R. Datta, U. V. Waghmare, and C. N. R. Rao, 2010 ACS Nano **4**, 1539.
- [4] D. Golberg, Y. Bando, Y. Huang, T. Terao, C. Tang, and C. Zhi, 2010 ACS Nano **4**, 2979.
- [5] M. L. Hu, Z. Z. Yu, K. W. Zhang, and L. Z. S. J. X. Zhong, 2011 J. Phys. Chem. C **115**, 8260.

- [6] K. S. Novoselov, A. K. Geim, S. V. Morozov, D. Jiang, Y. Zhang, S. V. Dubonos, I. V. Grigorieva, and A. A. Firsov, 2004 *Science* **306**, 666.
- [7] W. Q. Han, L. Wu, Y. Zhu, K. Watanabe, and T. Taniguchi, 2008 *Appl. Phys. Lett.* **93**, 223103.
- [8] C. Jin, F. Lin, K. Suenaga, and S. Iijima, 2009 *Phys. Rev. Lett.* **102**, 195505.
- [9] N. Alem, R. Erni, C. Kisielowski, M. D. Rossell, W. Gannett, and A. Zettl, 2009 *Phys. Rev. B* **80**, 155425.
- [10] L. Ci, L. Song, C. Jin, D. Jariwala, D. Wu, Y. L. A. Srivastava, Z. F. Wang, K. Storr, and L. Balicas, 2010 *Nat. Mater.* **9**, 430.
- [11] Y. Kobayashi, K.-I. Fukui, T. Enoki, K. Kusakabe, and Y. Kaburagi, 2005 *Phys. Rev. B* **71**, 193406.
- [12] Y. Niimi, T. Matsui, H. Kambara, K. Tagami, M. Tsukada, and H. Fukuyama, 2007 *Phys. Rev. B* **73**, 085421.
- [13] M. Topsakal, E. Akturk, and S. Ciraci, 2009 *Phys. Rev. B* **79**, 115442.
- [14] Z. Liu, L. Song, S. Zhao, J. Huang, J. Lou, and P. M. Ajayan, 2011 *Nano Lett.* **11**, 2032.
- [15] P. Sutter, R. Cortes, J. Lahiri, and E. Sutter, 2012 *Nano Lett.* **12**, 4869.
- [16] J. He, K. Q. Chen, Z. Q. Fan, L. M. Tang, and W. P. Hu, 2010 *Appl. Phys. Lett.* **97**, 193305.
- [17] L. Song, L. Balicas, D. J. Mowbray, R. B. Capaz, K. Storr, L. Ci, D. J., and S. K., 2012 *Phys. Rev. B* **86**, 075429.
- [18] J. C. Dong and H. Li, 2012 *J. Phys. Chem. C* **116**, 17259.
- [19] S. M.-M. Dubois, X. Declerck, J.-C. Charlier, and M. C. Payne, 2013 *ACS Nano*. **115**, 10836.
- [20] Y. Son, M. Cohen, and S. Louie, 2006 *Nature* **444**, 347.
- [21] S.-H. Ke, H. Baranger, and W. T. Yang, 2004 *Phys. Rev. B* **70**, 085401.
- [22] D. Sánchez-Portal, P. Ordejón, E. Artacho, and J. M. Soler, 1997 *J. Quantum Chem.* **65**, 453.
- [23] J. M. Soler, E. Artacho, J. D. Gale, A. Garcia, J. Junquera, P. Ordejón, and D. Sánchez-Portal, 2002 *J. Phys.:Condens. Matter* **14**, 2745.
- [24] N. Troullier and J. L. Martins, 1991 *Phys. Rev. B* **43**, 1993.
- [25] J. P. Perdew, K. Burke, and M. Ernzerhof, 1996 *Phys. Rev. Lett.* **77**, 3865.
- [26] S. M.-M. Dubois, Z. Zanolli, X. Declerck, and J.-C. Charlier, 2009 *Eur. Phys. J. B* **72**, 1.